Experiments in Fluids (2019) 60:22
https://doi.org/10.1007/s00348-018-2673-2

RESEARCH ARTICLE

Screech-tone prediction using upstream-travelling jet modes

Matteo Mancinelli[1,2] · **Vincent Jaunet**[1] · **Peter Jordan**[1] · **Aaron Towne**[3]

Received: 18 October 2018 / Revised: 19 December 2018 / Accepted: 21 December 2018

Abstract

The purpose of this paper is to characterise and model the A1 and A2 screech modes in supersonic jets operating at off-design conditions. The usual screech-modelling scenario involves a feedback loop between a downstream-travelling Kelvin–Helmholtz instability wave and an upstream-travelling acoustic wave. We review state-of-the-art screech-frequency prediction models and associated limitations. Following the work of Edgington-Mitchell et al. (J Fluid Mech 855, 2018), a new prediction approach is proposed where the feedback loop is closed by the upstream-travelling jet modes first discussed in Tam and Hu (J Fluid Mech 201:447–483, 1989) in lieu of the free-stream sound waves. The Kelvin–Helmholtz and upstream-travelling jet modes are obtained using a cylindrical vortex-sheet model. The predictions provide a better agreement with experimental observations than does the classical screech-prediction approach. Screech dynamics associated with the staging process is explored through a wavelet analysis, highlighting that staging involves mutually exclusive switching that is underpinned by non-linear interactions.

Graphical abstract

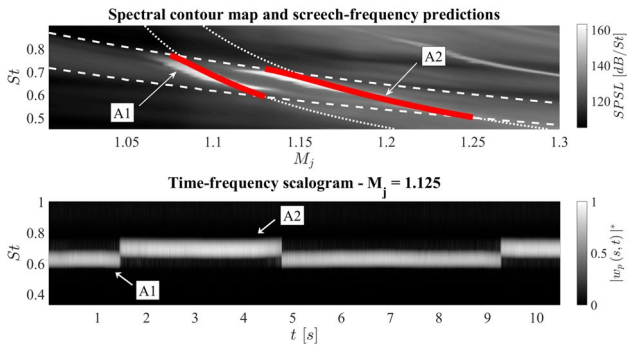

1 Introduction

Supersonic jets operating at off-design conditions include a shock-noise source in addition to the turbulent mixing noise that is usually dominant in subsonic and perfectly expanded supersonic jets. The shock-associated noise includes a broadband component and a tonal component known as screech (Tam 1995). Both are due to the interaction between the convected flow disturbances and the quasi-periodic shock-cell structure.

Screech has been broadly studied in the literature [see the review from Raman (1999)]. In his seminal work, Powell (1953) proposed a phenomenological description of the screech mechanism. He asserted that screech involves the interaction between downstream-travelling flow instabilities, which originate at the nozzle lip, and the shock-cell structure. This interaction was understood to generate acoustic waves that propagate back to the nozzle where they trigger new instabilities, thus closing the loop. Powell (1953), furthermore, showed how screech is characterised by different stages: the tone-frequency evolution with jet Mach

✉ Matteo Mancinelli
matteo.mancinelli@univ-poitiers.fr

Extended author information available on the last page of the article

Published online: 03 January 2019

number involves sudden frequency jumps that occur at given flow conditions. He detected four different stages, which he named modes A, B, C, and D. Later, Merle (1957) showed, using Schlieren visualizations, that the A mode could be divided into two sub-modes, A1 and A2. According to Powell et al. (1992), A1 and A2 are axisymmetric modes, B and D are sinuous or flapping modes, and C is a helical mode. The staging behaviour was studied by Walker and Thomas (1997) on a rectangular jet using a high-order spectral analysis. Screech staging was found to occur for jet-flow conditions where peaks of bi-coherence were found, the frequency jump being, thus, associated with non-linear interactions between the different modes. Wavelet transforms were used by Walker et al. (1997) to show that the staging behaviour in a rectangular supersonic jet can involve a coexistence of several modes. While different aspects of screech staging have been discussed in the literature and some models have been proposed to account for this in prediction schemes (Gao and Li 2010), a satisfactory explanation of why staging occurs is still lacking.

A complete understanding of screech dynamics is necessary for the development of screech-frequency prediction models. Powell's simple model (Powell 1953) is based on the propagation time of downstream-travelling disturbances from the nozzle to the shock, on one hand, and, on the other, the propagation time of a free-stream acoustic wave from the shock to the nozzle. A modified version of this model was obtained by Tam et al. (1986) by considering the screech as a special case of broadband shock-associated noise. In this formulation, the screech frequency is explicitly expressed as a function of the shock-cell wavelength. Later, Panda (1999) proposed a modification of Tam's model that includes the wavelength of the standing wave formed by the superposition of the downstream-travelling instability wave and the upstream-travelling acoustic wave. Comparison of predictions made using the foregoing models with experimental data has provided rough agreement. We here explore improvements that can be obtained by more correctly modelling the guided, upstream-travelling acoustic jet modes that Edgington-Mitchell et al. (2018) and Gojon et al. (2018) show to be active in closing the screech loop.

Recently, it has been shown how these modes explain weak, forced resonance observed in high-speed subsonic jets (Towne et al. 2017), resonance in impinging subsonic and supersonic jets (Tam and Ahuja 1990; Bogey and Gojon 2017), and high-amplitude tones observed when a subsonic jet grazes an edge, as in a jet–flap interaction (Jordan et al. 2018).

The idea that screech involves the guided, upstream-travelling jet modes evoked above was first suggested by Shen and Tam (2002), who claimed that the feedback loop of modes A1 and B was closed by free-stream acoustic waves, whereas the loop of modes A2 and C was closed by the acoustic jet modes. We here show that both the A1 and A2 modes are underpinned by resonance between downstream-travelling Kelvin–Helmholtz (K–H) instabilities and the said upstream-travelling jet modes. We do so by means of a novel linear screech-tone prediction model based on resonance between the aforesaid waves, and in this, we go beyond the work of Gojon et al. (2018) and Edgington-Mitchell et al. (2018), both of whom provided evidence that the guided modes underpin screech, without using this information to perform screech-frequency prediction.

Finally, using a wavelet transform of the measured pressure data, we show how the staging between A1 and A2 modes involves mutually exclusive switching between the two, and how this is underpinned by non-linear interactions. Given the success of the linear model which we use for tone-frequency prediction, this result demonstrates how non-linearity, whilst present and active in staging, and in the determination of screech amplitudes, does not have a strong impact on frequency selection.

The paper is organised as follows. A review of the previous screech-frequency prediction models as well as the presentation of the new approach involving the upstream-travelling jet waves are reported in Sect. 2. The experimental setup and the instrumentation adopted are described in Sect. 3, and the main results are presented in Sect. 4. Conclusions are finally discussed in Sect. 5.

2 Theoretical background

2.1 Screech-tone-frequency prediction models

Powell's original screech-prediction approach involves a downstream-travelling Kelvin–Helmholtz instability and an upstream-travelling free-stream acoustic wave (Powell 1953). With this assumption, the time taken for a flow disturbance to reach the reflection point (assumed to be the third or fourth shock cell) plus the time required for the resulting sound wave to travel back to the nozzle orifice can be written as follows:

$$T = \int \frac{\mathrm{d}h}{U_\mathrm{c}} + \frac{h}{c_\infty}, \tag{1}$$

where U_c and c_∞ are the convection velocity and the ambient speed of sound, respectively, and h is the spacing between the nozzle exhaust and the downstream reflection position. This model allows the screech frequency f_s to be written in terms of the number of cycles $\theta = N + p$ of the flow disturbance:

$$\frac{N+p}{f_\mathrm{s}} = \frac{h}{U_\mathrm{c}} + \frac{h}{c_\infty}, \tag{2}$$

where N and p are an integer and a constant, respectively. Tam et al. (1986) proposed the alternative version:

$$f_s = \frac{k_{sc} U_c}{2\pi\left(1 + \frac{U_c}{c_\infty}\right)}, \tag{3}$$

where k_{sc} is the shock-cell wavenumber. It is straightforward to show that Tam's formula is not very different from that obtained by Powell (1953) by considering that $k_{sc} = \frac{2\pi}{\lambda_{sc}}$, with λ_{sc} being the shock-cell wavelength, and $h = n\lambda_{sc}$. The screech-frequency formula can thus be written as follows:

$$\frac{n}{f_s} = \frac{h}{U_c} + \frac{h}{c_\infty}. \tag{4}$$

In the same work, Tam et al. (1986) also proposed a semi-empirical correction to Eq. (4) to account for temperature effects.

An alternative formulation has been proposed by Panda (1999), where the standing wave that occurs due to superposition of the downstream- and upstream-travelling waves is incorporated, leading to:

$$\frac{1}{\lambda_{sw}} = \frac{1}{\lambda_h} + \frac{1}{\lambda_a} = \frac{f_s}{U_c} + \frac{f_s}{c_\infty} \implies \frac{m}{f_s} = \frac{h}{U_c} + \frac{h}{c_\infty}, \tag{5}$$

where the substitution $h = m\lambda_{sw}$ has been performed to obtain an expression for the screech frequency as a function of the distance between the nozzle exit and the downstream reflection location. In all of the above formulae, the convection velocity is usually taken as a constant and included between 0.6 and 0.8 of the jet velocity U_j.

2.2 The resonance model

In this section, we present a screech-frequency prediction model that is based on a resonance between two waves travelling in opposite directions. We make predictions based on downstream-travelling Kelvin–Helmholtz waves and two kinds of upstream-travelling wave: (1) free-stream acoustic waves; (2) guided acoustic jet modes. Following Towne et al. (2017) and Jordan et al. (2018), we use the terms downstream- and upstream-travelling to designate the sign of the group velocity. Accordingly, the downstream-travelling modes are denoted with the superscript +, whereas the upstream-travelling modes are indicated with the superscript −. The notation used throughout the manuscript is reported in the following for the sake of clarity. The Kelvin–Helmholtz mode is denoted k_{KH}, the guided acoustic jet modes k_p, and the free-stream acoustic wave k_a.

2.2.1 Cylindrical vortex-sheet model

The linear dynamics of the waves are modelled using a cylindrical vortex-sheet (Lessen et al. 1965; Michalke 1970; Towne et al. 2017). Following the procedure used in Jordan et al. (2018), the normal mode ansatz is:

$$q(x, r, \theta, t) = \hat{q}(r) e^{i(kx + m\theta - \omega t)}, \tag{6}$$

where m is the order of the azimuthal mode, k is the streamwise wavenumber normalised by the nozzle diameter, D and ω is a non-dimensional frequency $\omega = 2\pi St M_a$, with $\mathrm{St} = fD/U_j$ the nozzle diameter-based Strouhal number and $M_a = U_j/c_\infty$ the acoustic Mach number. The vortex-sheet dispersion relation is:

$$D(k, \omega; M_a, T, m) = \frac{1}{\left(1 - \frac{kM_a}{\omega}\right)^2} + \frac{1}{T} \frac{I_m\left(\frac{\gamma_i}{2}\right)\left(\frac{\gamma_o}{2} K_{m-1}\left(\frac{\gamma_o}{2}\right) + m K_m\left(\frac{\gamma_o}{2}\right)\right)}{K_m\left(\frac{\gamma_o}{2}\right)\left(\frac{\gamma_i}{2} I_{m-1}\left(\frac{\gamma_i}{2}\right) - m I_m\left(\frac{\gamma_i}{2}\right)\right)} = 0, \tag{7}$$

with

$$\gamma_i = \sqrt{k^2 - \frac{1}{T}(\omega - M_a k)^2}, \tag{8a}$$

$$\gamma_o = \sqrt{k^2 - \omega^2}, \tag{8b}$$

where I and K are modified Bessel functions of the first kind and second kind, respectively, and T is the jet-to-ambient temperature ratio T_j/T_∞, so that the relation between the acoustic and jet Mach numbers is given by $M_j = U_j/c_j = M_a/\sqrt{T}$. We assume isothermal conditions in the modelling, that is $T = 1$.

Frequency/wavenumber pairs (ω, k) that satisfy Eq. (7) define eigenmodes of the vortex sheet for given values of m, M_a, and T. To find these pairs, we specify a real frequency ω and compute the associated eigenvalues k according to Eq. (7). It is straightforward to show that, because of the normalisation adopted, the free-stream acoustic wave is simply given by $k_a^{\pm} = \pm 2\pi St M_a$. The upstream-travelling guided jet waves belong to a hierarchical family of modes characterised by their azimuthal and radial order (m, j). We restrict attention to azimuthal mode $m = 0$ due to the axisymmetry property of screech modes A1 and A2. The radial order of the k_p waves is varied in the range $j = 1, 2$. Figure 1 shows an eigenspectrum comprising the k_{KH} and k_p modes for azimuthal mode $m = 0$. The acoustic wave, k_a^-, as well as a line with slope corresponding to a phase speed equal to $0.8\,U_j$, an approximation frequently made for the K–H mode, are also reported. As an example, we consider the jet-flow condition $M_j = 1.1$. We note the following features of the k_p^- jet modes. Unlike the acoustic waves, they are dispersive. They only exist as propagative waves in a narrow frequency band delimited by the branch- and saddle-points $B(m, j)$ and

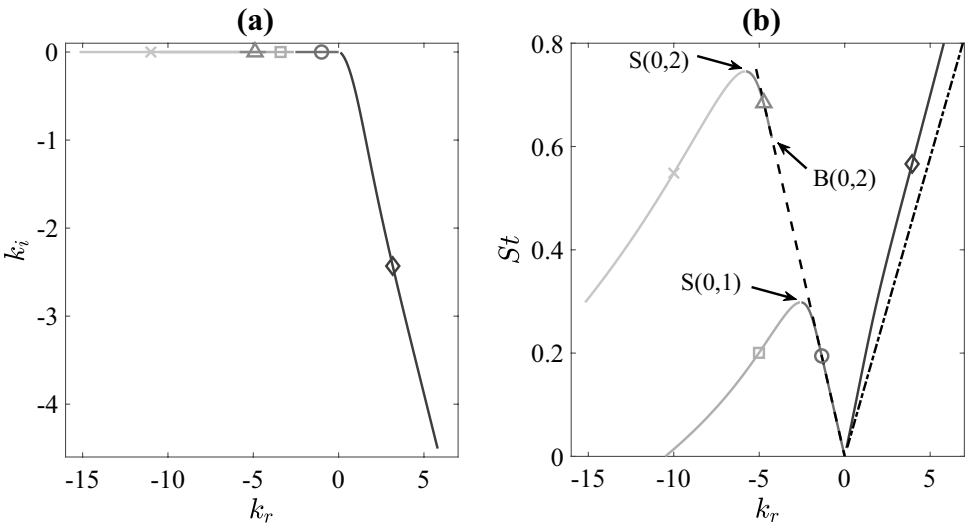

Fig. 1 Eigenvalues of the k_{KH} and k_p modes for the jet-flow condition $M_j = 1.1$ for azimuthal mode $m = 0$. $\diamond$ correspond to k^+_{KH}, $\circ$ to k^-_p for radial order $j = 1$, $\square$ to k^+_p for $j = 1$, $\triangle$ to k^-_p for $j = 2$, $\times$ to k^+_p for $j = 2$, dash–dotted line to a non-dispersive wave whose phase speed is $0.8\,U_j$, dashed line to free-stream acoustic wave. The branch- and saddle-points of the guided jet waves for each pair of (m, j) orders are indicated as well with letters B and S, respectively

$S(m, j)$, respectively. Their phase velocity is subsonic but very close to the speed of sound, particularly at the lower frequency end of the branch where the eigenvalues coincide almost exactly with those of free-stream sound waves. Furthermore, as pointed out by Tam and Ahuja (1990), the branch point $B(0, 1)$ for azimuthal mode $m = 0$ and radial order $j = 1$ in the $k_r - \mathrm{St}$ plane coincides with the origin. Finally, we note that the k^+_{KH} mode is slightly dispersive, and its phase velocity is a little higher than the usually adopted 0.6–0.8 U_j. These trends are consistent with the findings of Michalke (1984).

2.2.2 Resonance criteria

In this section, we discuss the conditions that the k^+ and k^- waves must satisfy in order for resonance to occur. Resonance can clearly only exist in the frequency range where both waves coexist and are propagative. It is, therefore, clear that, where the k^-_p guided jet modes are concerned, the eligible frequencies for resonance lie in the band delimited by the branch- and saddle-points, as the waves are evanescent outside of this range.

We assume that the waves exchange energy upstream at the nozzle exit, where the k^+_{KH} mode is generated, and at some downstream location, where a determinant interaction between the K–H mode and the shock-cell pattern occurs. This location is frequently considered to lie somewhere between the third and the fourth shock cells (Mercier et al. 2017). Hence, we can infer that the nozzle exit plane and a location around the third and fourth shock cells represent the end conditions for resonance. Following Pack (1950), the first shock-cell length is given by the following:

$$L_1(M_j) = \frac{\pi}{2.4048}\sqrt{M_j^2 - 1}. \tag{9}$$

Taking into account the shock-cell length decrease due to mixing layer growth, the sth shock-cell location is given by the following:

$$L_s(M_j) = L_1((1 - \alpha)s + \alpha), \tag{10}$$

where α is the rate of decrease of the shock-cell length with the downstream distance, and which takes a value of 0.06 according to Harper-Bourne (1974).

As reported by Jordan et al. (2018) (see also Landau and Lifshitz 2013), the conditions required for resonance involve both magnitude and phase constraints:

$$e^{\Delta k_i L_s} = |R_1 R_2|, \tag{11a}$$

$$\Delta k_r L_s + \phi = 2p\pi, \tag{11b}$$

where R_1 and R_2 are complex reflection coefficients at the boundaries, ϕ is the phase of the complex product $R_1 R_2$, and p is an integer. Following Jordan et al. (2018), we neglect the magnitude constraint, which is related to the imaginary part of the eigenvalues. The phase component relation (11b) then completely determines the resonance conditions. Given that the true phase of reflection is unknown, following Jordan et al. (2018), we explore the two extremes $\phi = 0$ and $\phi = \pi$, which lead to two resonance criteria:

$$k^+ - k^- = \Delta k_r = \frac{2p\pi}{L_s}, \tag{12a}$$

$$k^+ - k^- = \Delta k_r = \frac{(2p + 1)\pi}{L_s}. \tag{12b}$$

We consider resonance predictions by assuming the k^- wave active in resonance to be, on one hand, a free-stream sound wave, and, on the other, a guided jet mode. We allow the downstream reflection location to vary between the second and fifth shock cells. The best agreement was obtained

by considering downstream reflection to occur at the fourth shock cell, i.e., $s = 4$, which is consistent with the observations of Mercier et al. (2017). All results presented in what follows correspond to this value. In addition, the out-of-phase reflection condition (Eq. (12b)) provided best agreement with data, and so this is what is considered in the following analysis. Figure 2 illustrates the screech-frequency prediction for $M_j = 1.1$, considering resonant mode pair k^+_{KH}/k^-_p, Eq. (12b) and with $s = 4$.

3 Experimental setup

An experimental test campaign was performed at the *SUCRÉ* (SUpersoniC REsonance) jet-noise facility of the Institut Pprime in Poitiers. The fully anechoic chamber measures $3 \times 3 \times 2.5$ m^3 in size. The feed-line consists of a compressed dry-air duct at 200 bar. An electrically driven valve permits regulation of the jet velocity by controlling the pressure of the incoming flow. The inflow conditions are continuously monitored by a thermocouple and a pressure transducer which provide the stagnation temperature and pressure, respectively, at the inlet section of the nozzle. A heating system is installed to keep the stagnation temperature at the nozzle inlet constant and equal to 295 K. A settling chamber with a honeycomb panel and mesh grids is positioned upstream of the nozzle to have the desired inflow quality. The jet exit conditions are obtained by means of isentropic flow relations between the stagnation and ambient conditions at the nozzle exit. The supersonic under-expanded jet issues from a simple convergent nozzle of diameter $D = 0.01$ m. Experimental tests were carried out for a stagnation pressure range $p_0 = [1.89, 2.77]$ with the corresponding fully expanded jet Mach-number range $M_j = [1, 1.3]$ and a nozzle diameter-based Reynolds number range $Re = U_j D/\nu = [2.86 \times 10^5, 4.3 \times 10^5]$. The tests were performed with a very fine Mach-number resolution, $\Delta M_j = 0.005$, to capture the fine details of the Mach-number dependence of the screech tones.

Pressure fluctuations were measured by GRAS 46BP microphones, whose frequency response is flat in the range 4 Hz–70 kHz. Data were acquired by a National Instruments PXIe-1071 acquisition card with a sampling frequency of 200 kHz, which provides a maximum resolved Strouhal number range [2.6, 3.2] well above the St of interest in this paper. The acquisition time was set equal to 30 s, which is six orders of magnitude larger than the longest convective time, thus ensuring statistical convergence of the quantities presented in the paper. An azimuthal array of six microphones was placed in the nozzle exit plane and radial distance $r/D = 1$. Such a device allowed to resolve the most energetic azimuthal Fourier modes: $m = 0, \pm 1, \pm 2$. A schematic representation of the experimental setup and microphone disposition is depicted in Fig. 3.

Additional experiments were conducted in the far field to verify that the close proximity of the microphone array to the nozzle did not impact the screech dynamics. The results of this analysis are reported in Appendix 1.

4 Results

4.1 Screech-frequency prediction

Figure 4 shows the sound pressure spectrum level SPSL (Pierce and Beyer 1990), in dB/St, as a function of M_j for azimuthal mode $m = 0$. Specifically:

$$\mathrm{SPSL} = 10 \log_{10} \left(\frac{\mathrm{PSD}}{p^2_{\mathrm{ref}}} \frac{U_j}{D} \right), \tag{13}$$

where PSD is the power spectral density computed through the Welch's method and p_{ref} is the reference pressure, equal

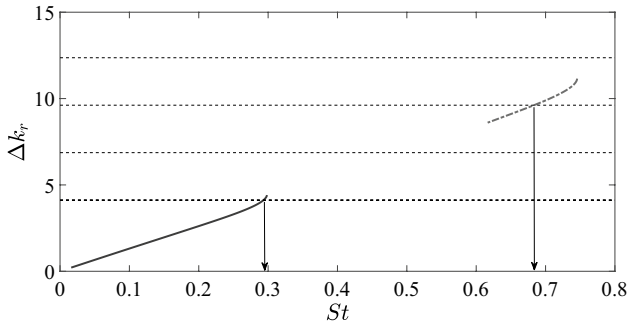

Fig. 2 Value of Δk between k^+_{KH} and k^-_p and identification of the resonance frequency for the jet Mach number $M_j = 1.1$ for azimuthal mode $m = 0$. Solid line refers to radial order $j = 1$, dash–dotted line to $j = 2$, and horizontal dashed lines to resonance criteria in the case of out-of-phase reflection condition

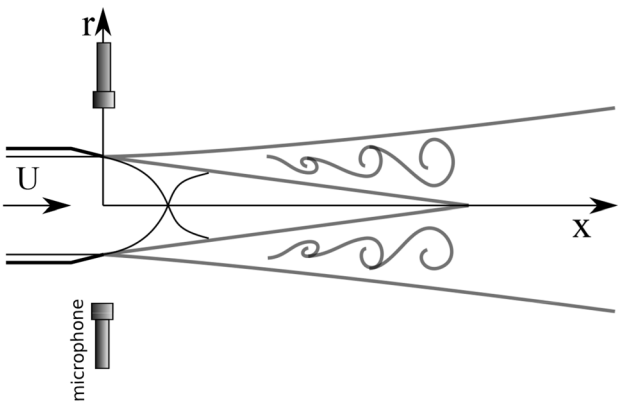

Fig. 3 Schematic representation of the experimental setup and microphone disposition

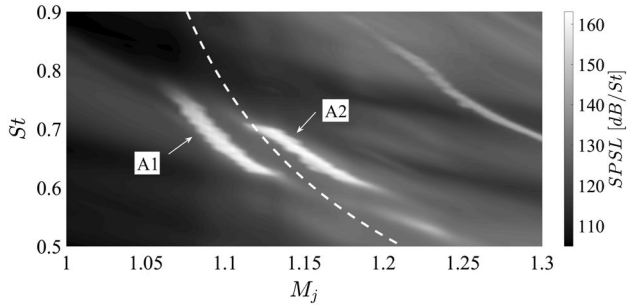

Fig. 4 Spectral contour map of azimuthal mode $m = 0$ and screech-frequency prediction using Tam's formula (4)

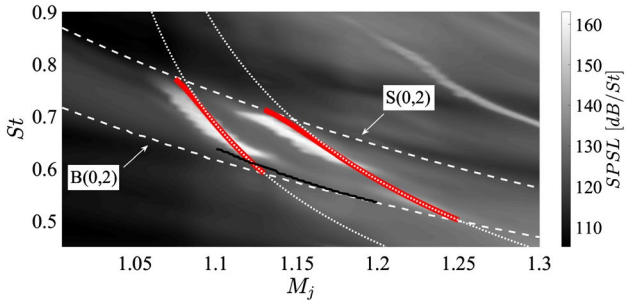

Fig. 5 Spectral contour map of azimuthal mode $m = 0$ and screech-frequency predictions using the resonance model presented in Sect. 2.2: white dotted lines refer to the prediction obtained using the free-stream sound waves k_a^- and red bold lines to the guided jet modes k_p^-. The branch- and saddle-point tracks $B(0, 2)$ and $S(0, 2)$ are indicated with white dashed lines. Black solid line refers to prediction obtained by Shen and Tam (2002) using the guided jet modes

to 20μPa. The signature of the A1 and A2 screech modes is clearly detectable as well as the mode switch that occurs in the vicinity of $M_j = 1.12$. The screech-frequency prediction obtained using Tam's formula (4) is superimposed on the plot. It provides only a very rough agreement with the experimental data, and the staging behaviour is not captured. Furthermore, the model predicts screech at Mach numbers and frequencies for which no tones are measured.

Screech-tone predictions obtained using the resonance model presented in Sect. 2.2 are shown in Fig. 5. Prediction using both the free-stream sound waves and the guided jet modes is shown. The k_p^- predictions are made assuming k_p^- modes of radial order $j = 2$ and values of p in Eq. (12b) equal to 3 and 4 for modes A1 and A2, respectively. A summary of the parameters used is reported in Table 1. Figure 5 shows, in addition to the screech-tone predictions, the branch- and saddle-point tracks of the guided jet modes. As recently discussed by Edgington-Mitchell et al. (2018) and Gojon et al. (2018), the screech tones of both modes A1 and A2 are bounded by the branch- and saddle-points. The cut-off and cut-on frequencies of screech are thus explained by the fact that the guided jet waves, k_p^-, are evanescent outside the $\mathrm{St} - M$ region defined by the $B(0, 2)$ and $S(0, 2)$ tracks. This is in contrast to the model involving free-stream sound waves which predicts screech tones for $\mathrm{St} - M$ regions where tones are not observed. Furthermore, the guided-jet-mode screech model provides a better description of the screech-tone Mach-number dependence in the vicinity of the high-frequency cut-off for both the A1 and A2 modes.

Table 1 Summary of the parameters adopted to obtain screech-frequency predictions

Mode	m	Shock cell	Reflection condition	p	j of k_p^-
A1	0	4	Out-of-phase	3	2
A2	0	4	Out-of-phase	4	2

We also include the predictions of Shen and Tam (2002) using the k_p^- modes. The authors claimed that mode A1 was underpinned by a free-stream sound wave, and mode A2 by a guided jet mode. Figure 5 shows that their prediction agrees poorly with the experimental data.

To sum up, a linear, vortex-sheet model has been used to provide screech-tone predictions of modes A1 and A2 using upstream-travelling guided jet waves as the closure mechanism. The predictions provide a better agreement with experiments than does the usual approach based on free-stream sound waves. In the next section, we explore non-linear aspects of the staging dynamics of screech modes A1 and A2.

4.2 Staging dynamics

We perform a time–frequency analysis to explore the screech dynamics associated with the staging process. This is achieved via a wavelet transform of the pressure signal $p(t)$ (Farge 1992; Mancinelli et al. 2017). This provides wavelet coefficients which are a function of time, t, and of scale, s, which is inversely proportional to the frequency. The Continuous Wavelet Transform (CWT) is given by the following (Mancinelli et al. 2017),

$$w(s,t) = C_\psi^{-1/2} s^{-1/2} \int_{-\infty}^{+\infty} p(\tau) \Psi^* \left(\frac{t-\tau}{s} \right) \mathrm{d}\tau, \tag{14}$$

where $\Psi^*\left(\frac{t-\tau}{s}\right)$ is the complex conjugate of the dilated and translated mother wavelet $\Psi(t)$ which satisfies the admissibility condition (Meneveau 1991):

$$C_\psi = \int_{-\infty}^{+\infty} \left|\hat{\Psi}(\omega)\right|^2 \frac{\mathrm{d}\omega}{\omega} < \infty, \tag{15}$$

where ω is the angular frequency. The CWT was computed using a complex bump wavelet kernel, whose expression in the Fourier domain is (Jiang and Suter 2017):

$$\hat{\Psi}(\omega) = \left(e^{1-\frac{1}{1-\sigma^2(\omega-\mu)^2}}\right)F(\omega), \tag{16}$$

$$F(\omega) = \begin{cases} 1 & \text{if } \mu - \frac{1}{\sigma} \le \omega \le \mu + \frac{1}{\sigma} \\ 0 & \text{else} \end{cases}, \tag{17}$$

where μ and σ are parameters chosen to have the desired frequency resolution and time localisation (Jordan et al. 2018).

To explore the screech dynamics in the staging process, we focus on flow conditions where the switch from mode A1 to A2 occurs, i.e., $M_j = 1.115$, 1.12, 1.125, and 1.13. Figure 6 shows the time–frequency scalogram for these jet Mach numbers, and the amplitude of the wavelet coefficients has been normalised by the maximum amplitude at each wavelet scale/frequency. Frequency is expressed in terms of St and the plot shows only the first 10 s of the acquisition, that is five orders of magnitude larger than the characteristic flow time scale (the results do not change for the other time lapses). For $M_j = 1.115$ (and, in general, up to this flow condition), only the screech frequency associated with mode A1 is detected. As M_j increases to the value of 1.12, jumps occur between modes A1 (St_1) and A2 (St_2). The jumps are mutually exclusive. As the jet Mach number is further increased ($M_j = 1.125$), the time lapses over which the mode A2 appears become larger. For $M_j = 1.13$ (and, in general, beyond this flow condition), only the component St_2 is detected, the screech having definitively switched to mode A2. We emphasize that the two modes A1 and A2 are mutually exclusive. No coexistence of the two modes was observed, in contrast to the observations of Shen and Tam (2002) and Walker et al. (1997) in a rectangular jet.

Finally, we consider the jet-flow condition $M_j = 1.125$, where the mutually exclusive mode switching was most evident. We extract the time evolution of the amplitude of the wavelet coefficients corresponding to the screech frequency of mode A1, i.e., $St_1 = 0.63$. We then compute the PSD of $|w_p(St_1, t)|$, which is shown in semi-logarithmic scale in Fig. 7. The *PSD* has been normalised multiplying by U_j/D and dividing by p^2_{ref}. We observe that the amplitude is modulated at a Strouhal number $St_d \approx 0.069$, which is close to the difference frequency between that of mode A2 $St_2 = 0.7$ and that of mode A1 $St_1 = 0.63$. This indicates that a quadratic, non-linear interaction occurs between modes A1 and A2. Indeed, the weak presence of the St_d component can also be observed in the pressure spectrum of azimuthal mode $m = 0$ for the same flow condition $M_j = 1.125$, as shown in Fig. 8. We point out that the St_d component appears in the pressure spectra only for the jet Mach numbers where the switch from mode A1 and A2 occurs, thus confirming that switching is underpinned by non-linear dynamics. This result supports that of Walker and Thomas (1997), that the staging process is an inherently non-linear process. Further analysis is necessary to more satisfactorily clarify the nature of the non-linear dynamics.

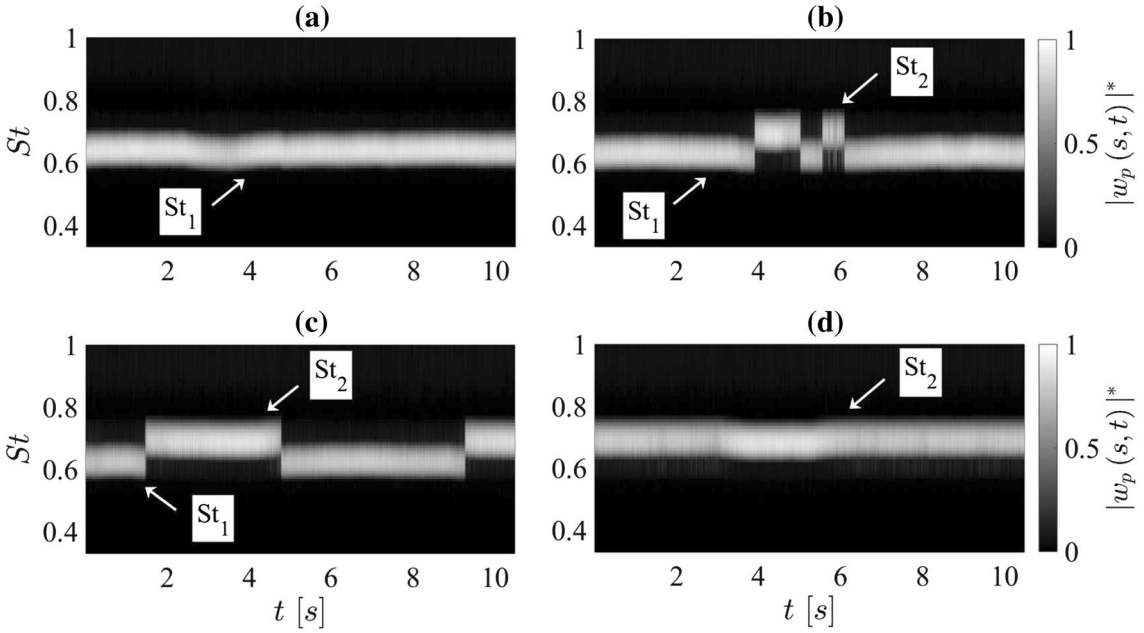

Fig. 6 Time–frequency scalogram for the jet Mach numbers: **a** $M_j = 1.115$, **b** $M_j = 1.12$, **c** $M_j = 1.125$, and **d** $M_j = 1.13$. The screech frequencies related to modes A1 and A2 are indicated as St_1 and St_2, respectively

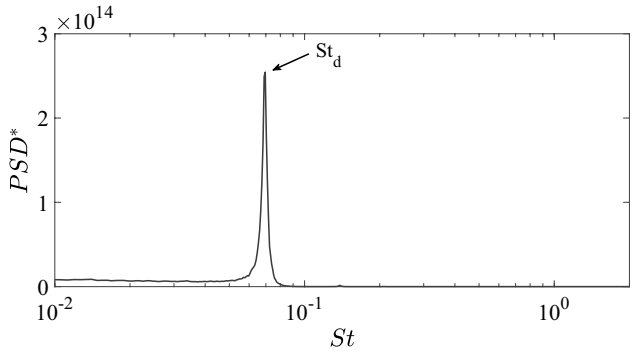

Fig. 7 Normalised power spectral density of the time evolution of the amplitude of the wavelet coefficient at the scale/frequency corresponding to the screech frequency of mode A1

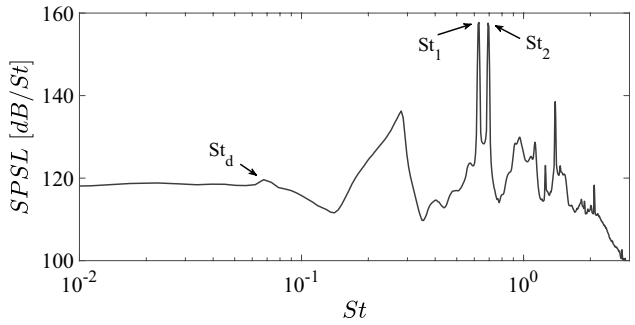

Fig. 8 Pressure spectrum of azimuthal mode $m = 0$ for jet Mach number $M_j = 1.125$

5 Conclusions

The screech of a supersonic jet issuing from a simple convergent nozzle has been characterised and modelled. Near-field pressure measurements were performed at the nozzle exhaust using an azimuthal array for jet-flow conditions typical of the axisymmetric screeching modes A1 and A2. The main contribution is a new approach, following Jordan et al. (2018), for screech-frequency prediction, on one hand, and, on the other, a time–frequency analysis of the staging process that indicates its underpinning by non-linear dynamics. Despite the role played by non-linearities in mode switching, the linear modelling framework for screech-frequency predictions that we propose captures the evolution of screech with jet Mach number for both modes A1 and A2. This suggests that non-linearity, while present, is not important for frequency selection.

A critical review of the state-of-the-art screech-prediction models has been carried out underlining their limitations. A novel approach for the prediction of the screech frequency is proposed in the framework of the resonance between downstream-travelling Kelvin–Helmholtz wavepackets and upstream-travelling, guided jet modes. Both were computed using a cylindrical vortex-sheet model. The resulting prediction is in closer agreement with the experimental data than what is obtained by assuming the upstream-travelling component of the screech loop to comprise free-stream acoustic waves. The screech tones of both modes A1 and A2 only occur in the frequency-Mach-number region, bounded by the branch- and saddle-point tracks, where the upstream-travelling guided jet modes are propagative.

A time–frequency analysis using wavelet transform was performed to explore the screech dynamics associated with the staging process. The time–frequency scalogram of azimuthal mode $m = 0$ showed that the A1 and A2 modes are mutually exclusive during staging. We observed, furthermore, that the amplitude of the wavelet coefficients at the scale/frequency corresponding to mode A1 is modulated at the difference frequency between modes A1 and A2. This behaviour suggests a quadratic, non-linear interaction between A1 and A2 modes during staging.

Acknowledgements M. M. acknowledges the support of Centre National d'Études Spatiales (CNES) under a post-doctoral grant.

Appendix 1: Far-field measurements

Pressure measurements were performed in the far field to verify that the screech dynamics of modes A1 and A2 was not affected by the close positioning of the near-field microphone array with respect to the nozzle. The far-field microphone was placed at a radial distance $r/D \approx 90$ at a polar position $\psi = 120°$, with the polar angle measured from the downstream axis of the jet. A coarser jet Mach-number resolution $\Delta M_j = 0.01$ was used to carry out the far-field experimental tests.

Figure 9 shows the spectral contour map for all M_j. As for the near-field measurements, we restrict the attention on the frequency band where modes A1 and A2 live. The signature of the two modes is the same one arising in the near field

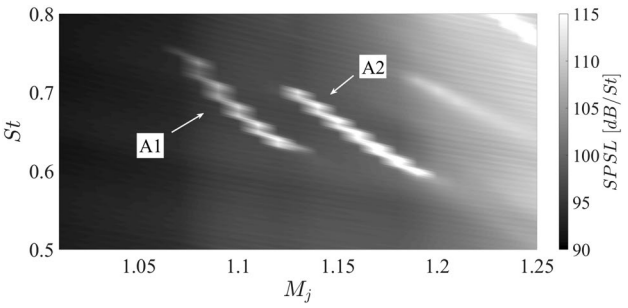

Fig. 9 Spectral contour map of the far-field microphone at the polar position $\psi = 120°$

and shown in Figs. 4 and 5. Hence, the close positioning of the microphone array in the near field has no effects on the emergence of the axisymmetric screech modes.

References

Bogey C, Gojon R (2017) Feedback loop and upwind-propagating waves in ideally expanded supersonic impinging round jets. J Fluid Mech 823:562–591

Edgington-Mitchell D, Jaunet V, Jordan P, Towne A, Soria J, Honnery D (2018) Upstream-travelling acoustic jet modes as a closure mechanism for screech. J Fluid Mech. https://doi.org/10.1017/jfm.2018.642

Farge M (1992) Wavelet transforms and their applications to turbulence. Annu Rev Fluid Mech 24(1):395–458

Gao J, Li X (2010) A multi-mode screech frequency prediction formula for circular supersonic jets. J Acoust Soc Am 127(3):1251–1257

Gojon R, Bogey C, Mihaescu M (2018) Oscillation modes in screeching jets. AIAA J 56(7):1–7

Harper-Bourne M (1974) The noise from shock waves in supersonic jets-noise mechanism. Agard Cp-131 11:1–13

Jiang Q, Suter BW (2017) Instantaneous frequency estimation based on synchrosqueezing wavelet transform. Signal Process 138:167–181

Jordan P, Jaunet V, Towne A, Cavalieri AVG, Colonius T, Schmidt O, Agarwal A (2018) Jet-flap interaction tones. J Fluid Mech 853:333–358

Landau LD, Lifshitz EM (2013) Course of theoretical physics. Elsevier, Amsterdam

Lessen M, Fox JA, Zien HM (1965) On the inviscid stability of the laminar mixing of two parallel streams of a compressible fluid. J Fluid Mech 23(2):355–367

Mancinelli M, Di Marco A, Camussi R (2017a) Multivariate and conditioned statistics of velocity and wall pressure fluctuations induced by a jet interacting with a flat plate. J Fluid Mech 823:134–165

Mancinelli M, Pagliaroli T, Di Marco A, Camussi R, Castelain T (2017b) Wavelet decomposition of hydrodynamic and acoustic pressures in the near field of the jet. J Fluid Mech 813:716–749

Meneveau C (1991) Analysis of turbulence in the orthonormal wavelet representation. J Fluid Mech 232:469–520

Mercier B, Castelain T, Bailly C (2017) Experimental characterisation of the screech feedback loop in underexpanded round jets. J Fluid Mech 824:202–229

Merle M (1957) Nouvelles recherches sur les fréquences ultrasonores émises par les jets d'air. In: Ann. Télécommun, vol 12. Springer, pp 424–426

Michalke A (1970) A note on the spatial jet-Instability of the compressible cylindrical vortex sheet. Technical report, DLR

Michalke A (1984) Survey on jet instability theory. Prog Aerosp Sci 21:159–199

Pack DC (1950) A note on prandtl's formula for the wave-length of a supersonic gas jet. Q J Mech Appl Math 3(2):173–181

Panda J (1999) An experimental investigation of screech noise generation. J Fluid Mech 378:71–96

Pierce AD, Beyer RT (1990) Acoustics: an introduction to its physical principles and applications, 1989 edn. Acoustical Society of America, New York

Powell A (1953) On the mechanism of choked jet noise. Proc Phys Soc Lond Sect B 66:1039

Powell A, Umeda Y, Ishii R (1992) Observations of the oscillation modes of choked circular jets. J Acoust Soc Am 92(5):2823–2836

Raman G (1999) Supersonic jet screech: half-century from powell to the present. J Sound Vib 225(3):543–571

Shen H, Tam CKW (2002) Three-dimensional numerical simulation of the jet screech phenomenon. AIAA J 40(1):33–41

Tam CKW (1995) Supersonic jet noise. Annu Rev Fluid Mech 27(1):17–43

Tam CKW, Ahuja KK (1990) Theoretical model of discrete tone generation by impinging jets. J Fluid Mech 214:67–87

Tam CKW, Hu FQ (1989) On the three families of instability waves of high-speed jets. J Fluid Mech 201:447–483

Tam CKW, Seiner JM, Yu JC (1986) Proposed relationship between broadband shock associated noise and screech tones. J Sound Vib 110(2):309–321

Towne A, Cavalieri AVG, Jordan P, Colonius T, Schmidt O, Jaunet V, Brès GA (2017) Acoustic resonance in the potential core of subsonic jets. J Fluid Mech 825:1113–1152

Walker SH, Thomas FO (1997) Experiments characterizing nonlinear shear layer dynamics in a supersonic rectangular jet undergoing screech. Phys Fluids 9(9):2562–2579

Walker SH, Gordeyev SV, Thomas FO (1997) A wavelet transform analysis applied to unsteady aspects of supersonic jet screech resonance. Exp Fluids 22(3):229–238

Affiliations

Matteo Mancinelli[1,2] · Vincent Jaunet[1] · Peter Jordan[1] · Aaron Towne[3]

Vincent Jaunet
vincent.jaunet@ensma.fr

Peter Jordan
peter.jordan@univ-poitiers.fr

Aaron Towne
towne@umich.edu

[1] Département Fluides Thermique et Combustion, Institut Pprime-CNRS-Université de Poitiers-ENSMA, 11 Boulevard Marie et Pierre Curie, 86962 Chasseneuil-du-Poitou, Poitiers, France

[2] Direction des Lanceurs, CNES, 52 rue Jacques Hillairet, 75612 Paris, France

[3] Department of Mechanical Engineering, University of Michigan, 2350 Hayward Street, Ann Arbor, MI 48109, USA